

Contents lists available at ScienceDirect

Materials Today: Proceedings

journal homepage: www.elsevier.com/locate/matpr



Composite mesoporous SiO₂-Al₂O₃ supported Fe, FeCo and FeRu catalysts for Fischer-Tropsch studies in a 3-D printed stainless-steel microreactor

S. Bepari^a, R. Stevens-Boyd^b, N. Mohammad^b, Xin Li^a, R. Abrokwah^a, D. Kuila^{a,b}

ARTICLE INFO

Article history: Received 16 February 2020 Received in revised form 18 April 2020 Accepted 21 April 2020 Available online 29 May 2020

Keywords:
Mesoporous composite-oxide support
Fischer-Tropsch (FT)
Ruthenium (Ru)
Cobalt (Co)
Iron (Fe) Stainless Steel microreactor
H₂-TPR
Catalysts

ABSTRACT

Composite oxide support, $SiO_2-Al_2O_3$, with high surface area, was prepared by one-pot procedure, and 10 wt%Fe, 10%Fe5%Co, and 10%Fe5%Ru were impregnated for Fischer-Tropsch (FT) studies. BET studies show the hysteresis loop for mesoporous (m) structure of the composite. H_2 -TPR studies showed the effect of Ru and Co on iron oxide reduction at lower temperature and XPS studies confirmed two oxidation states for cobalt and iron with different binding energies. The FT studies in a 3D printed stainless steel (SS) microchannel microreactor were performed at 1 atm at 300 °C. 10Fe5Ru catalyst showed better CO conversion and higher selectivity to C_1 - C_3 hydrocarbons.

© 2020 Elsevier Ltd. All rights reserved.

Selection and Peer-review under responsibility of the scientific committee of the International Conference on Nanomaterials for Energy, Environment and Sustainability.

1. Introduction

The rapid development of fuel economy is gaining attention in producing liquid hydrocarbons from sources other than coal, such as biomass, biogas and CO₂, etc. Fischer-Tropsch (FT) synthesis is one of the alternative procedures to produce liquid hydrocarbons or value-added chemicals from syngas (a mixture of CO and H₂) which is produced from carbon-containing materials (e.g. natural gas, biogas and biomass) via partial oxidation [1], steam reforming [2] or auto-thermal reforming [3]. FT synthesis is a very important route also for conversion of gas to liquid (GTL) fuels. The GTL technology is considered to be economically profitable by pearl GTL project, a collaboration between Shell and Qatar petroleum, with productivity of 140,000 bpd (barrels per day) [4]. The major issue in such a large-scale GTL process is to meet the demand that is economical for production in an industry [5]. Microreactor technology is a very promising route to meet this challenge; different catalytic processes have been investigated by researchers in academia and corporations such as Velocvs and Micromeritics [6-8]. Furthermore, the synthesis of a suitable catalyst in terms of product yield and stability will also play a major role in the economics of FT synthesis. Iron, cobalt and ruthenium are well known catalysts for FT synthesis; however, ruthenium due to its limitation in resources and high cost is usually used as a promoter and rarely used as a catalyst. Iron, due to its low cost and ability to produce hydrogen through water-gas shift reaction (WGS), is the most suitable catalyst for wide range of operating temperatures without losing the catalyst activity over time on stream [9–11]. Thus, for FT synthesis with low syngas (H₂/CO) ratio, Fe based catalysts is more advantageous [9,12]. Several studies have also reported that iron is the ideal catalyst for high temperature FTS (HT-FTS: 300-350 °C) to produce C₂-C₄ olefins and C5+ hydrocarbons, and low temperature FT (LT-FTS: 200-280 °C) for selective C₅₊ productions [13-15]. FT synthesis with Fe based catalysts in many conventional reactor systems i.e. fixed bed reactor (FBR), micro-fixed bed reactor, slurry phase CSTR (Continuous Stirred tank reactor) have been studied extensively [16-18]. In our previous work, we used Simicroreactors for FT studies with monometallic Fe, Co, and Ru and bimetallic FeCo catalysts supported by silica [19,20], alumina [21] and TiO₂ [13]. In addition, we carried out F-T studies with Co-Ru bimetallic catalysts in 3-D printed SS microreactor using different mesoporous silica support [14]. However, F-T studies in SS microchannel microreactor coated with Fe based catalysts has not been extensively investigated. In this study, an one-pot

E-mail address: dkuila@ncat.edu (D. Kuila)

^a Department of Chemistry, Applied Sciences and Technology, North Carolina A&T State University, Greensboro, NC 27411, USA

b Department of Nanoengineering, Joint School of Nanoscience and Nanoengineering, North Carolina A&T State University, Greensboro, NC 27411, USA

synthesis procedure was used to explore any synergistic effect of the support in the m-SiO₂-Al₂O₃ composite containing metal catalysts. The catalysts were characterized by BET, H₂-TPR, SEM, XPS and XRD techniques to study the physiochemical properties of the materials and understand the unique interaction between the metals and the mixed oxide support. More specifically, the FT performance of Fe based catalysts, in the presence of Co and Ru, in composite mesoporous SiO₂-Al₂O₃ support in a 3-D printed microchannel microreactor was investigated.

2. Experimental

2.1. Catalyst preparation

The composite oxide support was prepared using a one-pot procedure [22,23]. All the catalysts are denoted as 10Fe/m-SiO₂-Al₂O₃, 10Fe5Co/m-SiO₂-Al₂O₃ and 10Fe5Ru/m-SiO₂-Al₂O₃ (where m stands for mesoporous and 10 M means 10 wt% of the respective metal and 5 M corresponds to 5 wt%). The molar composition of the reagents used was: 1 TEOS: 0.589 CoH21O3Al: 0.081 CTAB: 41 H₂O: 7.5 ethanol: 0.0167 Pl23: 5.981 HCl. For typical synthesis, first P123 was dissolved in 2 M HCl at 35 °C to obtain a clear solution designated as solution "A". A second solution designated as "B" was prepared by dissolving CTAB in DI water and stirring at 35 °C until a colourless solution was obtained. Solution B was then gently poured into solution A while stirring for 30 min to obtain mixture C. In a separate beaker, C₉H₂₁O₃Al was dissolved in ethanol and heated at 80 °C until complete dissolution. The dissolved C₉H₂₁O₃Al was added to TEOS and stirred rigorously to prevent precipitation and was designated solution 'D'. Solution D, which was quite viscous was then added dropwise to the mixture 'C' and stirred vigorously. This final mixture was covered with parafilm and stirred for 20 h at 35 °C for aging under the fume hood. The final aqueous mixture with pH = 1.5 was then aged at 80 °C in the oven for at least 48 h (to dry) followed by air-drying under fume hood for 24 h. The sample (now a greyish precipitate) was then oven-dried again for 24 h at 98 °C. Finally, the dried material was calcined in a furnace under air at 550 °C for 6hrs.

Iron (III) nitrate nonahydrate (Fe (NO₃)₃·9H₂O 99%), cobalt (II) nitrate hexahydrate (Co (NO₃)₂·6H₂O), ruthenium chloride (RuCl₃·xH₂O) were the metal precursors used for the synthesis of catalysts. The metals were immobilized on the support via wetimpregnation method. A 5 wt% loading of Co or Ru was used with 10 wt% Fe. After impregnation, the catalyst was dried overnight at 90 °C in an oven. Finally, it was calcined in a furnace at 400 °C for 5 h.

2.2. Microreactor fabrication

Additive manufacturing technology was used to fabricate the microchannel microreactor and its cover channel. The reactor was designed using an AutoCAD software and printed using metal sintering 3D printing process. The reactor comprised of 11 microchannels as a reaction zone, each channel is $500\,\mu\text{m}\times500\,\mu\text{m}\times2.4\,\text{cm}.$ The reactor is fixed in a custom-built heating block with inlet and outlet channels which allows the entry of syngas into the reaction zone and exit of the gaseous products into the in-line GC [14].

2.3. Catalyst loading on microreactor

The microchannels of the 3D printed stainless-steel microreactor were dip coated with catalyst slurry (solution of catalyst, PVA, DI water and acetic acid) followed by sonication and drying in air.

The microreactor was then calcined at $450\,^{\circ}\text{C}$ for $6\,\text{h}$ to remove PVA and the volatiles.

2.4. Catalyst activity test

F-T reactions were performed in an in-house built microreactor set up as shown in our previous work [13]. Operation parameters like feed flowrate, pressure and temperature were controlled by LabVIEW software. Hydrogen and carbon monoxide gases were passed to the reactor block system through a stainless steel piping along with an ultrapure nitrogen line connected to the downstream of the reactor to move the products into the Gas Chromatography-Mass Spectrometer (Agilent GCMS, 7890B GC and 5977A MSD) for quantitative analysis. Mass flow controllers (Cole-Parmer MFC 32907-51) were used to adjust the flow rates of CO and H₂ using the software. The hydrogen and carbon monoxide MFCs had a maximum setting of 1 ml/min while the nitrogen MFC has a maximum setting of 10 ml/min. Heating tapes were wrapped around the upstream and downstream reactor lines to insulate and preheat the reactant gases to keep them in the gaseous phase. CO conversion and hydrocarbon selectivity were calculated based on the following equations [13,14]:

$$X_{CO}(\%) = \frac{F_{CO,in} - F_{CO,out}}{F_{CO,in}} \times 100$$
 (1)

$$\textit{CH}_{4} \, \textit{Selectivity} \, (\%) \, = \frac{\textit{mCH}_{4}}{\textit{mCH}_{4} + 2 \textit{mC}_{2} \textit{H}_{6} + 3 \textit{mC}_{3} \textit{H}_{8}} \times 100 \tag{2} \label{eq:2}$$

$$C_{2}H_{6}\,Selecti\,vity\,(\%)\,=\frac{2mC_{2}H_{6}}{mCH_{4}+2mC_{2}H_{6}+3mC_{3}H_{8}}\times100 \eqno(3)$$

$$C_{3}H_{8}\,Selectivity\,(\%)\,=\frac{3mC_{3}H_{8}}{mCH_{4}+2mC_{2}H_{6}+3mC_{3}H_{8}}\times 100 \eqno(4)$$

where, F represents the molar flow rate for CO in ml/min.

2.5. Catalyst characterization

Surface and pore analysis were conducted by a Micromeritics 3Flex instrument under N_2 adsorption/desorption. 0.2 g of sample was degassed using Micromeritics Smart Vac unit at 150 °C for 5 h. The surface area was calculated using the Bruner-Emmett-Teller equation within the p/p_0 range of 0.05 to 0.31.

Temperature programmed reduction was performed using a Micromeritics 3Flex analyzer. A typical sample, 0.05 g of the material was weighed and placed into a chemisorption tube on the top of a covering layer of quartz wool beneath a quartz filter cap. The sample was then placed under an H_2/Ar (1:9 wt%) flow of 110.34 ml/min and a ramp rate of 10 °C/min from room temperature to 1000 °C to determine reducibility of the metal oxides.

All the materials were imaged with a ZEISS Auriga Focused Ion Beam Scanning Electron Microscope (FIBSEM) at the Joint School of Nanoscience and Nanoengineering. These images were used to draw conclusions of the average particle size, morphology and topography of each catalyst.

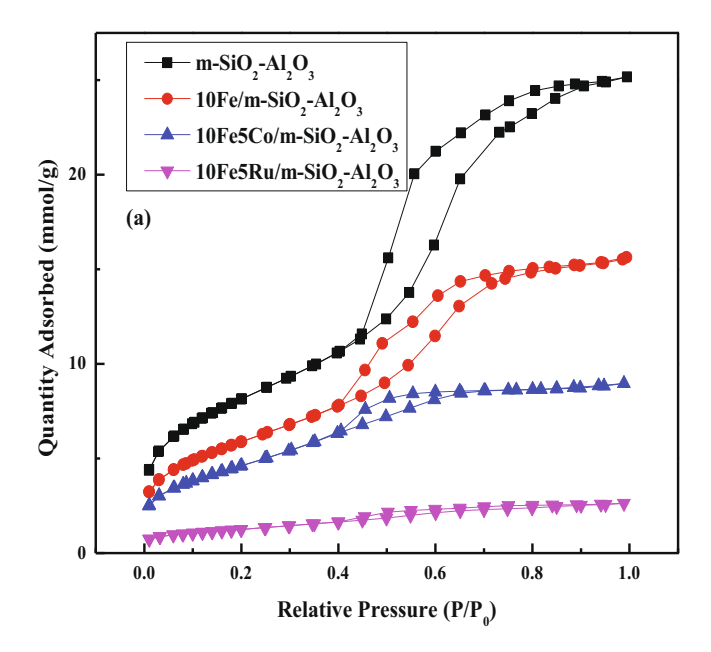
Powder XRD studies were performed using an X-ray diffractometer (Bruker AXS). The detection limit of the instrument fell between a 2θ value of $20\text{-}80^\circ$ with a step interval of 0.02° using a Cu K α 1 radiation source with a wavelength of 1.5406 Å. Peaks observed in the spectra were used to identify the catalyst metals, their oxidation state, and morphology.

The oxidation states of the metals were analysed by X-ray photon spectroscopy (XPS-Escalab Xi+-Thermo scientific).

3. Results and discussion

3.1. Textural properties of catalysts

The BET isotherms and pore size distribution curves of parent mesoporous SiO₂-Al₂O₃ (m-SiO₂-Al₂O₃) and all metal impregnated catalysts are shown in Fig. 1(a). The BET surface area, pore diameter and pore volume of all catalysts are presented in Table 1. The isotherms of m-SiO₂-Al₂O₃ and 10Fe/ m-SiO₂-Al₂O₃ samples exhibited type IV behaviour according to IUPAC classifications [23,24]. The H1 hysteresis loop nature of the isotherms confirm the presence of uniform cylindrical pores [23], with a pore size distribution of 3 nm to 6 nm depicted in Fig. 1(b). As shown in Table 1, the bare m-SiO₂-Al₂O₃ showed the highest surface area, pore diameter and the total pore volume. However, incorporation of Fe, Ru and Co resulted in a decline of these textural parameters. This suggests partial blocking of the pores by the added metals as evidenced



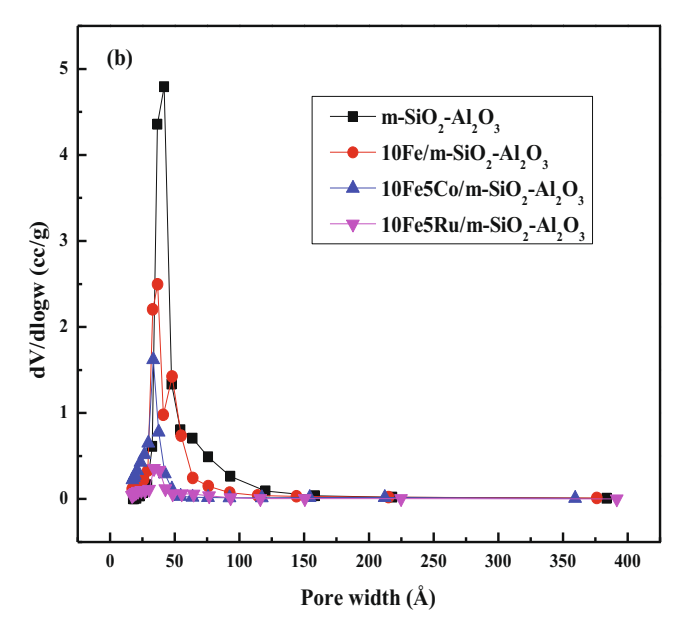


Fig. 1. (a) Nitrogen physisorption isotherms, (b) Pore size distribution calculated using BJH method for m-SiO₂-Al₂O₃ and metal-impregnated m-SiO₂-Al₂O₃.

Table 1Textural properties of mixed mesoporous support (m-SiO₂-Al₂O₃) and metal-impregnated catalysts.

Catalyst	BET surface area (m^2/g)	Pore diameter (nm)	Pore volume (cc/g)
m-SiO ₂ -Al ₂ O ₃	654.78	5.33	0.873
10Fe/m-SiO ₂ -Al ₂ O ₃	479.27	4.52	0.542
10Fe5Co/m-SiO ₂ -Al ₂ O ₃	382.63	3.25	0.311
10Fe5Ru/m-SiO ₂ -Al ₂ O ₃	101.67	3.58	0.091

by the narrowing of the hysteresis loop of the isotherms in Fig. 1 (a).

3.2. H₂-TPR studies

Temperature programmed reduction (TPR) analysis was performed to investigate the reduction attributes of the metal oxides and how they interacted with the mixed mesoporous support. Fig. 2 shows the reduction profiles for all catalysts. In case of the 10Fe/m-SiO₂-Al₂O₃ catalyst, the lower temperature peak around 370 °C can be attributed to reduction of Fe_2O_3 to Fe_3O_4 [25]. The second peak around 620 °C corresponds to reduction of Fe₃O₄ to FeO [25]. The third peak around 780 °C can be assigned to reduction of FeO to Fe. The low-temperature peak is normally attributed to bulk iron oxide that is well dispersed over the support, and it can be reduced easily [26]. However, the higher temperature reduction peak is due to iron oxide which interacted strongly with the support [26]. The TPR profile of bimetallic catalysts contains several overlapping peaks, making it difficult to predict the exact reduction behaviour of two metals. For 10Fe5Co/m-SiO₂-Al₂O₃ catalyst, the two distinct peaks between 300 °C and 410 °C correspond to reduction of Co₃O₄ to CoO and CoO to Co⁰ respectively [27,28]. Fe₂O₃ is also reduced to yield Fe₃O₄ at 300 °C. Incorporation of Co can facilitate reduction of Fe₃O₄ to FeO at lower-temperature around 480 °C [29]. At a higher temperature between 800 and 1000 °C, the broad peak corresponds to reduction of small cobalt and/or iron oxide particles [30]. In the case of 10Fe5Ru/m-SiO₂-Al₂O₃ catalyst, the reduction peak around 185 °C is due to reduction of RuO₂ to Ru⁰ [31,32]. This RuO₂ is not bound with Fe. The other peak around 235 °C is attributed to reduction of a small amount of RuO₂ present in bimetallic catalysts, i.e. associated with Fe (but not due to Fe) [33]. For all catalysts, consumed H_2 can be quantified and they are shown in Table 2.

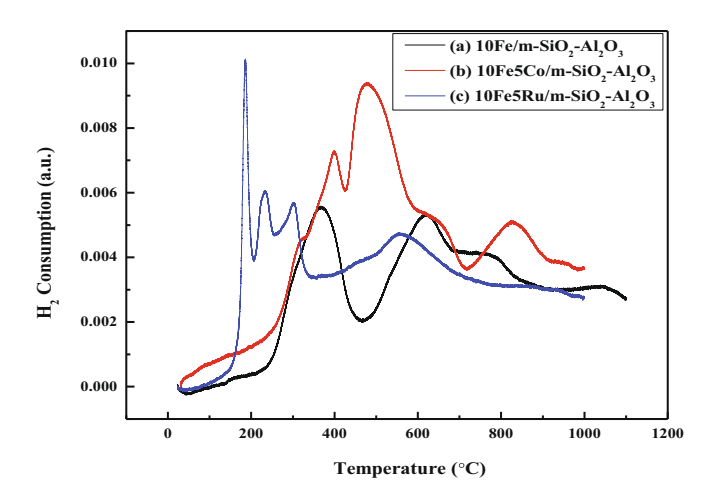


Fig. 2. H₂-TPR analyses of different catalysts: (a) 10Fe/m-SiO₂-Al₂O₃, (b) 10Fe5Co/m-SiO₂-Al₂O₃ and (c) 10Fe5Ru/m-SiO₂-Al₂O₃.

Table 2 H_2 consumption of $10Fe/m-SiO_2-Al_2O_3$, $10Fe5Co/m-SiO_2-Al_2O_3$ and $10Fe5Ru/m-SiO_2-Al_2O_3$ catalysts from TPR studies.

Catalyst	H ₂ consumption (μmol/g)		
10Fe/m-SiO ₂ -Al ₂ O ₃	66		
10Fe5Co/m-SiO ₂ -Al ₂ O ₃	120		
10Fe5Ru/m-SiO ₂ -Al ₂ O ₃	94		

The highest hydrogen consumption observed in FeCo/m-SiO $_2$ -Al $_2$ O $_3$ catalyst suggest that incorporation of Co in Fe/m-SiO $_2$ -Al $_2$ O $_3$ facilitates reduction of metals and they can be available for FT synthesis.

3.3. SEM-EDX analysis

The SEM images of all catalysts are shown in Fig. 3. Fig. 3(a) shows the SEM image of mesoporous bimetallic support oxide. The particles are well distributed with very little agglomeration. Fig. 3(b-c) shows small particles on the support which are basically Fe, Co, and Ru. The changes in the morphology of the support was observed with incorporation of metal/metals. Large non-uniform particles were observed both in FeCo/m-SiO₂-Al₂O₃ and FeRu/m-SiO₂-Al₂O₃ catalysts.

Fig. 4 shows the EDX spectra of the support and all catalysts. Table 3 shows the EDX results of all the elements in the catalysts. The wt.% of each metal after impregnation is almost equal to intended metal loading. After metal incorporation, the wt% of Al and Si in the support decreases for all metal impregnated catalysts.

3.4. XRD analysis

Fig. 5(A) shows the small-angle XRD patterns of all the catalysts and support. A diffraction peak due to mesoporous structure, cor-

responds to the (220) ($2\theta = 1.10^{\circ}$) plane [34]. The mesoporous support and impregnated samples exhibit similar characteristic peaks, indicating mesoporous structure has been conserved after incorporation of Fe, Co, and Ru metals. The wide-angle XRD patterns of the catalysts are shown in Fig. 5(B). No clear signals of metals can be observed in both Fe and FeCo catalysts. This suggests higher dispersion and small particle sizes of the metals [35]. For FeRu catalyst, the diffraction peaks of tetragonal RuO₂ (JCPDS-21-1172) are observed at 27.8°, 34.8° and 53.9° that correspond to (110), (101) and (211) crystal planes respectively [31]. The intensity of X-ray diffraction depends on the degree of crystallinity suggesting that ruthenium oxides exhibited the highest crystallinity in the composite oxide framework. As reported elsewhere, and shown here, the formation of well-defined RuO₂ crystals depend on calcination temperature and an optimum temperature of 400 °C is observed [36]. Nucleation of metal oxides during calcination is controlled by a supersaturation mechanism which is a function of factors like calcination temperature, pH and reactant concentration [37].

3.5. XPS analysis

The chemical oxidation states of iron, cobalt and ruthenium in mixed oxide SiO_2 - Al_2O_3 support were determined by XPS measurements. Fig. 6 shows the core level XPS spectra of Si-2p, Al-2p and O-1 s orbital electrons with a maximum binding energy of 101 eV, 73.6 eV and 531 eV, respectively. This confirms the presence of aluminosilicates in the mesoporous framework. The binding energy of the core electrons in the Fe, Co and Ru active sites in three catalysts show their transition states and are listed in Table 4. The XPS spectra for Fe 2p in all the three catalysts are shown in Fig. 7. Deconvolution of peaks into Fe $2p_{3/2}$ and Fe $2p_{1/2}$ with a small satellite peak are observed for FeCo/m-SiO₂-Al₂O₃ and Fe/m-SiO₂-Al₂O₃ samples. The shift in the peaks for the

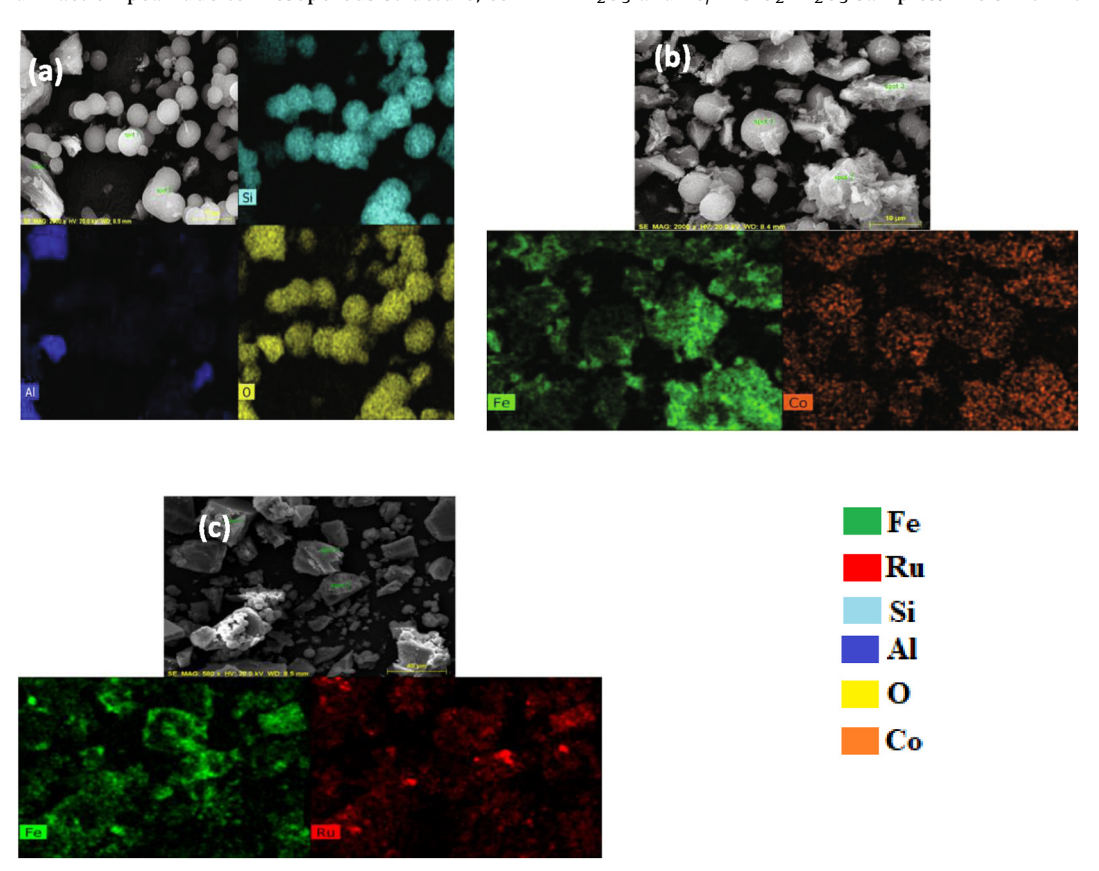
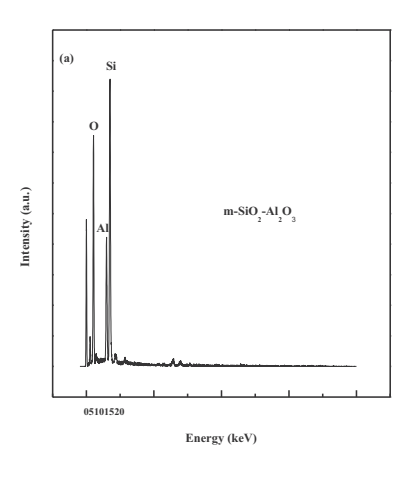
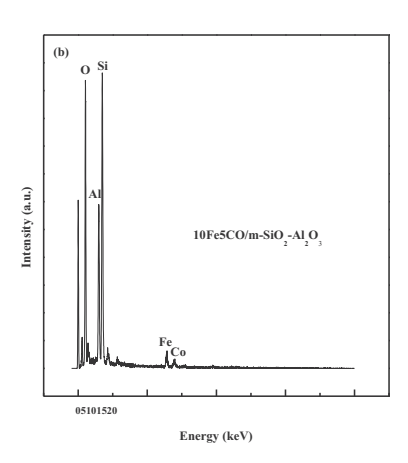


Fig. 3. SEM images and elemental mapping of the support and catalysts: (a) m-SiO₂-Al₂O₃; (b) 10Fe5Co/m-SiO₂-Al₂O₃; (c) 10Fe5Ru/m-SiO₂-Al₂O₃.





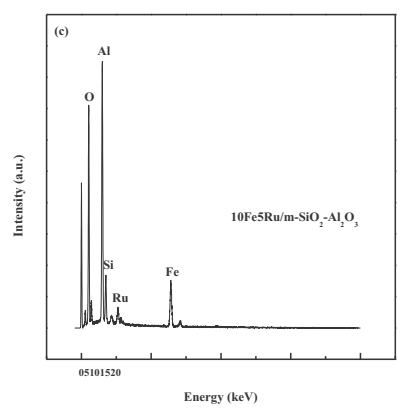


Fig. 4. EDX spectra of the support and catalysts: (a) m-SiO₂-Al₂O₃; (b) 10Fe5Co/m-SiO₂-Al₂O₃; (c) 10Fe5Ru/m-SiO₂-Al₂O₃.

Table 3 EDX analyses of mixed mesoporous support (m-SiO₂-Al₂O₃) and metal-impregnated catalysts.

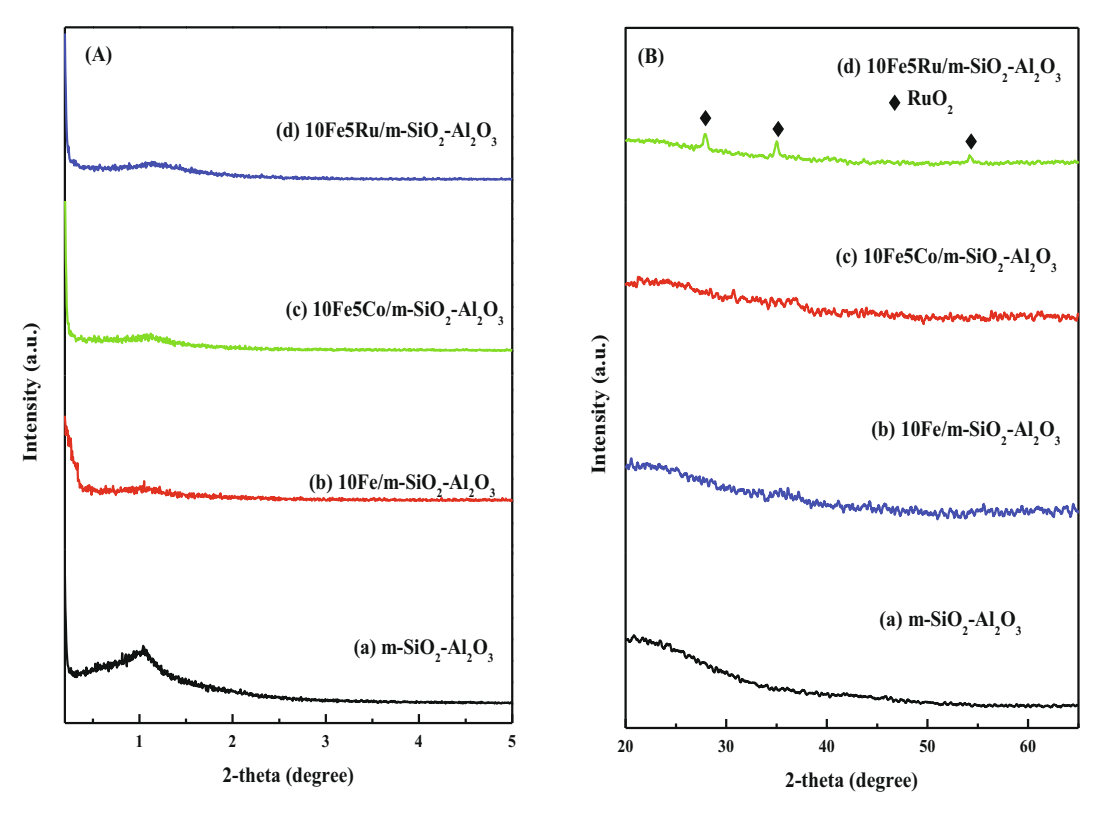
Catalyst	Metal loading (wt.%)					
	Si	Al	0	Fe	Co	Ru
m-SiO ₂ -Al ₂ O ₃	27.45	19.42	53.13	=	=	-
10Fe/m-SiO ₂ -Al ₂ O ₃	26.42	10.86	52.29	9.25		
10Fe5Co/m-SiO ₂ -Al ₂ O ₃	25.37	13.04	48.49	8.94	4.15	
10Fe5Ru/m-SiO ₂ -Al ₂ O ₃	20.33	17.85	47.10	10.54	_	6.26

different catalysts, in Table 4, show the differences in the metal and support interactions in different catalysts [14,38]. The presence of Ru is confirmed by Ru 3d spectra which is centred almost at 284 eV in FeRu/m-SiO₂-Al₂O₃. The cobalt 2p spectra also deconvoluted into Co $2p_{1/2}$ and Co $2p_{3/2}$ are clearly noticed in FeCo/m-SiO₂-Al₂O₃ [Fig. 7(b)].

3.6. Catalyst activity test

The performance of H_2 -reduced metal-supported catalysts for FT reaction at 300 °C and 1 atm is shown in Table 5. Only Febased catalyst showed maximum CO conversion. As surface area decreased due to incorporation of Co and Ru with Fe, which lead to less availability of active sites in the catalysts, Co and Ru incorporated catalysts showed less CO-conversion compared to the Fe catalyst only. Fe based catalyst only produced CH_4 with high selectivity. The other product, CO_2 is produced due to high activity of Fe in the water gas shift reaction. After the addition of Co to Fe, methane selectivity to CO_2 is reduced, and some amount of ethane

is produced. This result reflects that addition of Co facilitates Fe dispersion. H₂-TPR results also showed that the reducibility of Fe based catalyst increased with Co-incorporation. This trend is consistent with that reported by Iglesia et al. [39]. They showed that the FT reaction rates are proportional to metal dispersion and probably independent of the support. The same type of behavior is observed for the FeRu catalyst. They also showed that the FT reaction rate is proportional to the number of exposed Ru surface atoms and independent of crystallite size, support and metalsupport interactions [39]. Thus, incorporation of Ru increased distribution of Fe and reduced iron oxides to Fe at a lower temperature. While methane selectivity decreased, ethane selectivity slowly increased. A small amount of propane is observed under our reaction conditions. Iglesia et al. [40] explained the beneficial effect of Ru to be a cleansing effect during FT synthesis due to high CO hydrogenation ability which prevented the carbon formation over the catalyst surface. Table 5 shows that FeRu catalyst exhibited better selectivity compared to other catalysts under the same process conditions.



 $\textbf{Fig. 5.} \ \ (A) \ \ Small \ \ angle \ \ XRD \ \ angle \ \ XRD \ \ of \ \ mesoporous \ \ composite \ \ support \ \ and \ \ all \ \ catalysts \ (*) \ [*Fe/m-SiO_2-Al_2O_3; FeCo/m-SiO_2-Al_2O_3; FeRu/m-SiO_2-Al_2O_3].$

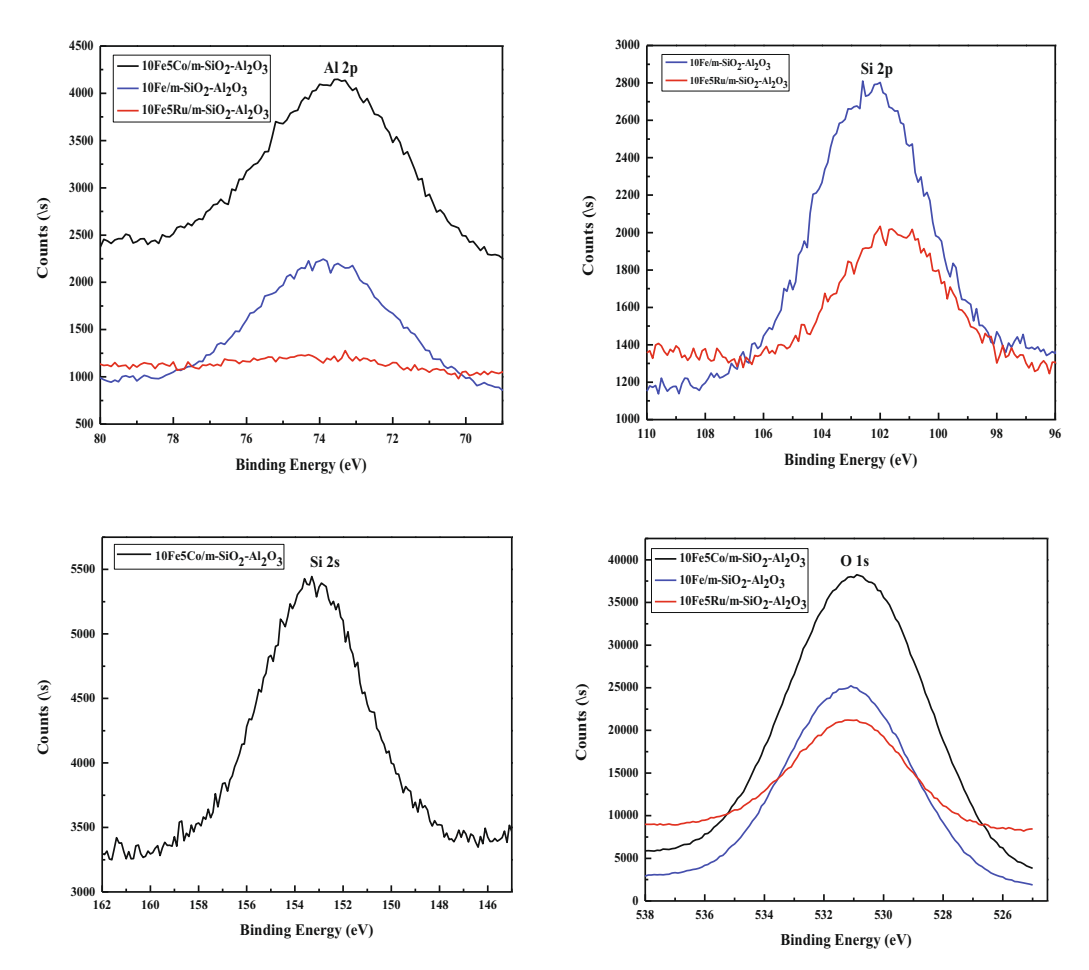
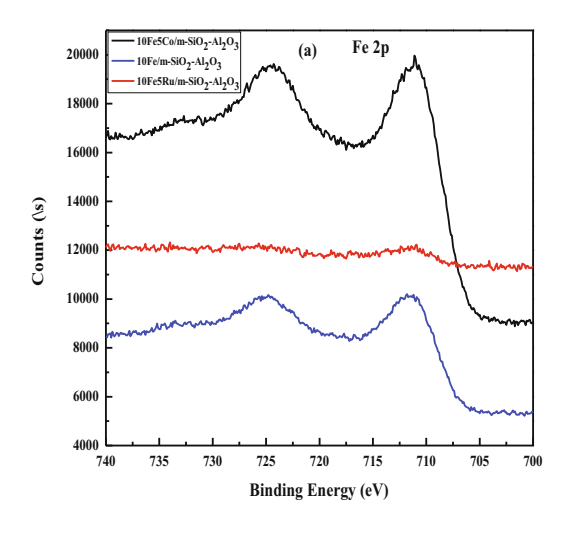
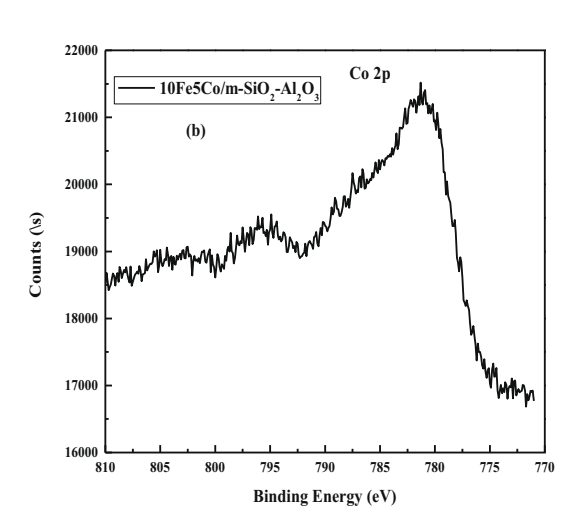


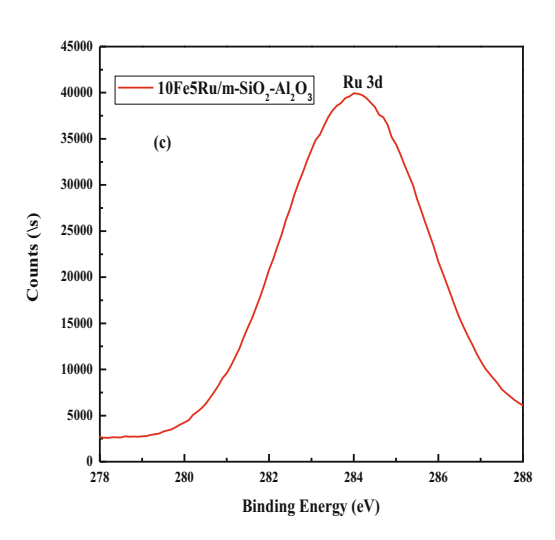
Fig. 6. Core levels XPS spectra of Si2p, Al2p and O1s in mesoporous support (m-SiO₂-Al₂O₃) and metal-impregnated catalysts.

Table 4Binding energy of the core electrons in the Fe, Ru and Co active sites in three catalysts.

Catalyst	Co 2p _{1/2}	Co 2p _{3/2}	Ru 3d _{3/2}	Fe 2p _{3/2}	Fe 2p _{1/2}
10Fe/m-SiO ₂ -Al ₂ O ₃ 10Fe5Co/m-SiO ₂ -Al ₂ O ₃	796 eV	781.2 eV		725.2 eV 724.4 eV	711.4 eV 711.2 eV
10Fe5Ru/m-SiO ₂ -Al ₂ O ₃			284 eV	725.3 eV	711.5 eV







 $\textbf{Fig. 7.} \ \ \textbf{XPS spectra of Fe2p, Co2p and Ru3d in (a) Fe/m-SiO_2-Al_2O_3; (b) FeCo/m-SiO_2-Al_2O_3; (c) FeRu/m-SiO_2-Al_2O_3 catalysts.$

Table 5 Performance of all FT catalysts at 300 °C.

Catalyst	CO conversion (%)	CH4 selectivity (%)	C2H6 selectivity (%)	C3H8 selectivity (%)	CO2 selectivity (%)
10Fe/m-SiO ₂ -Al ₂ O ₃	96.03	76.52	-	-	23.48
10Fe5Co/m-SiO ₂ -Al ₂ O ₃	62.44	9.65	1.66	_	88.7
10Fe5Ru/m-SiO ₂ -Al ₂ O ₃	70.94	32.97	14.82	2.22	49.98

4. Conclusions

All the catalysts were prepared by one-pot hydrothermal method for the composite support followed by wet impregnation for metal incorporation. The results from H₂-TPR and SEM analyses confirmed that mesoporous composite support (SiO₂-Al₂O₃) improved dispersion of Fe and the dispersion was further enhanced by incorporation of Co and Ru. The presence of Co and Ru improved selectivity towards formation of ethane and propane. The selectivity to methane was reduced after the addition of Co and Ru to Fe.

The overall performance of FeRu enhanced the selectivity of ethane and propane when compared to that of FeCo catalyst. Thus, the presence of Ru has a remarkable promoting effect on the catalytic performance of Fe/m-SiO₂-Al₂O₃ for FT synthesis.

CRediT authorship contribution statement

S. Bepari: Data curation, Methodology, Writing - original draft, Software. **R. Stevens-Boyd:** Data curation. **N. Mohammad:** Visualization, Investigation. **Xin Li:** Writing - review & editing.

R. Abrokwah: Conceptualization. **D. Kuila:** Supervision, Writing - review & editing.

Declaration of Competing Interest

The authors declare that they have no known competing financial interests or personal relationships that could have appeared to influence the work reported in this paper.

Acknowledgements

This work is performed at North Carolina A&T State University and Joint School of Nanoscience and Nanoengineering, (a member of the Southeastern Nanotechnology Infrastructure Corridor (SENIC) and National Nanotechnology Coordinated Infrastructure (NNCI) which is supported by NSF (Grant ECCS-1542174). The authors acknowledge the funding received from NSF CREST (#260326) and UNC-ROI (#110092).

References

- [1] A.T. Ashcroft, A.K. Cheetham, J.S. Foord, M.L.H. Green, C.P. Grey, A.J. Murrell, Nature 344 (1990) 319–321.
- [2] J.R. Rostrup-Nielsen, J. Catal. 85 (1984) 31-43.
- [3] J.R. Rostrup-Nielsen, Catal. Today 18 (1993) 305-324.
- [4] D.A. Wood, C. Nwaoha, B.F. Towler, J. Nat. Gas Sci. Eng. 9 (2012) 196-208.
- [5] Y. Sun, Z. Jia, G. Yang, L. Zhang, Z. Sun, Int. J. Hydrogen Energ. 42 (2017) 29222– 29235.
- [6] Y. Sun, G. Yang, L. Zhang, Z. Sun, Chem. Eng. Process 119 (2017) 44-61.
- [7] S.R. Deshmukh, A.L.Y. Tonkovich, K.T. Jarosch, L. Schrader, S.P. Fitzgerald, D.R. Kilanowski, J.J. Lerou, T.J. Mazanec, Ind. Eng. Chem. Res 49 (2010) 10883–10888.
- [8] L.C. Almeida, O. Sanz, J. Dolhaberriague, S. Yunes, M. Montes, Fuel 110 (2013) 171–177.
- [9] D.H. Chun, J.C. Park, S.Y. Hong, J.T. Lim, C.S. Kim, H.-T. Lee, J.-I. Yang, S. Hong, H. Jung, J. Catal. 317 (2014) 135–143.
- [10] X. Yu, J. Zhang, X. Wang, Q. Ma, X. Gao, H. Xia, X. Lai, S. Fan, T.-S. Zhao, Appl. Catal. B 232 (2018) 420–428.
- [11] Q. Zhang, J. Kang, Y. Wang, ChemCatChem 2 (2010) 1030–1058.
- [12] E. VanSteen, M. Claeys, K.P. Moller, D. Nabaho, Appl. Catal. A 549 (2018) 51–59.

- [13] R.Y. Abrokwah, M.M. Rahman, V.G. Deshmane, D. Kuila, Mol. Catal. 478 (2019) 110566.
- [14] N. Mohammad, S. Bepari, S. Aravamudhan, D. Kuila, Catalysts 9 (2019) 872.
- [15] S. Saeidi, M. Nikoo, A. Mirvakili, S. Bahrani, N.A. Saidina Amin, M.R. Rahimpour, Rev. Chem. Eng. 31 (2015) 209–238.
- [16] M. Sarkari, F. Fazlillahi, H. Ajamein, H. Atashi, W.C. Hecker, L.L. Baxter, Fuel Process. Technol. 127 (2014) 163–170.
- [17] F.G. Botes, J.W. Niemantsverdriet, J.A. van de Loosdrecht, Catal. Today 215 (2013) 112–120.
- [18] S. Chambrey, P. Fongarland, H. Karaca, S. Piche, A. Griboval-Constant, D. Schweich, F. Luck, S. Savin, A.Y. Khodakov, Catal. Today 171 (2011) 201–206.
- [19] S. Mehta, V. Deshmane, S. Zhao, D. Kuila, Ind. Eng. Chem. Res. 53 (2014) 16245–16253.
- [20] S. Zhao, V.S. Nagineni, N.V. Seetala, D. Kuila, Ind. Eng. Chem. Res. 47 (2008) 1684–1688.
- [21] V.S. Nagineni, S. Zhao, A. Potluri, Y. Liang, U. Siriwardane, N.V. Seetala, J. Fang, J. Palmer, D. Kuila, Ind. Eng. Chem. Res. 44 (2005) 5602–5607.
- [22] A. Vinu, V. Murugesan, W. Bolhlmann, M. Hartmann, J. Phys. Chem. B 108 (2004) 11496–11505.
- [23] H.M. Gobara, Egypt. J. Pet. 21 (2012) 1-10.
- [24] A. Corma, M.T. Navarro, J.P. Parienté, J. Chem. Soc. ChemComm (1994) 147–148
- [25] P. Sirikulbodee, T. Ratana, T. Sornchamni, M. Phongaksorn, S. Tungkamani, Energy Procedia 138 (2017) 998–1003.
- [26] R. Brown, M.E. Cooper, D.A. Whan, Appl. Catal. 3 (1982) 177-186.
- [27] Z. Shang-hong, S. Hai-quan, D. Ning, Y. Shi-yong, L. Ke-wei, J. Fuel Chem. Technol. 42 (2014) 449–454.
- [28] A. Lapidus, A. Krylova, V. Kazanskii, V. Borovkov, A. Zaitsev, Appl. Catal. 73 (1991) 65–82.
- [29] A. Biabani-Ravandi, M. Rezaei, Chem. Eng. J. 184 (2012) 141-146.
- [30] A. Griboval-Constant, A. Butel, V.V. Ordomsky, P.A. Chernavskii, A.Y. Khodakov, Appl. Catal. A 481 (2014) 116–126.
- [31] T. Huo-qiang, L. Jin-lin, J. Fuel Chem. Technol. 39 (2011) 615-620.
- [32] M. Nurunnabi, K. Murata, K. Okabe, M. Inaba, I. Takahara, Appl. Catal. A 340 (2008) 203–211.
- [33] L. Guczi, Z. Schay, K. Matusek, I. Bogyay, Appl. Catal. 22 (1986) 289-309.
- [34] X. Liu, B. Tian, C. Yu, F. Gao, S. Xie, B. Tu, R. Che, L.-M. Peng, D. Zhao, Angew. Chem. Int. Ed. 41 (2002) 3876–3878.
- [35] L. Han, D. Mao, J. Yu, Q. Guo, G. Lu, Catal. Commun. 23 (2012) 20-24.
- [36] Y. Li, L.A. Zhang, Y. Qin, F. Chu, Y. Kong, Y. Tao, Y. Li, Y. Bu, D. Ding, M. Liu, ACS. Catal. 8 (2018) 5714–5720.
- [37] F. Meshkani, M. Rezaei, Chem. Eng. J. 260 (2015) 107–116.
- [38] N. Mohammad, R.Y. Abrokwah, R.G. Stevens-Boyd, S. Aravamudhan, D. Kuila, Catal. Today (2020), https://doi.org/10.1016/j.cattod.2020.02.020.
- [39] E. Iglesia, S.L. Soled, R.A. Fiato, J. Catal. 137 (1992) 212–224.
- [40] E. Iglesia, S.L. Soled, R.A. Fiato, G.H. Via, J. Catal. 143 (1993) 345-368.